On the Structure and Desorption Dynamics of DNA Bases Adsorbed on Gold: A Temperature-Programmed Study

Mattias Östblom and Bo Liedberg*

Division of Molecular Physics, Department of Physics, Chemistry and Biology, Linköping University, S-581 83 Linköping, Sweden

Linette M. Demers and Chad A. Mirkin

Department of Chemistry and Center for Nanofabrication and Molecular Self-Assembly, Northwestern University, 2145 Sheridan Road, Evanston, Illinois 60208

Received: March 30, 2005; In Final Form: June 2, 2005

The structure and desorption dynamics of mono- and multilayer samples of adenine, cytosine, guanine, and thymine on polycrystalline gold thin films are studied using temperature-programmed desorption−infrared reflection absorption spectroscopy (TPD-IRAS) and temperature-programmed desorption−mass spectroscopy (TPD-MS). It is shown that the pyrimidines, adenine and guanine, adsorb to gold in a complex manner and that both adhesive (adenine) and cohesive (guanine) interactions contribute the apparent binding energies to the substrate surface. Adenine displays at least two adsorption sites, including a high-energy site (210 °C, ∼136 kJ/mol), wherein the molecule coordinates to the gold substrate via the NH_2 group in an sp^3-like, strongly perturbed, nonplanar configuration. The purines, cytosine and thymine, display a less complicated adsorption/desorption behavior. The desorption energy for cytosine (160 °C, ∼122 kJ/mol) is similar to those obtained for adenine and guanine, but desorption occurs from a single site of dispersed, nonaggregated cytosine. Thymine desorbs also from a single site but at a significantly lower energy (100 °C, ∼104 kJ/mol). Infrared data reveal that the monolayer architectures discussed herein are structurally very different from those observed for the bases in the bulk crystalline state. It is also evident that both pyrimidines and purines adsorb on gold with the plane of the molecule in a nonparallel orientation with respect to the substrate surface. The results of this work are discussed in the context of improving the understanding of the design of capturing oligonucleotides or DNA strands for bioanalytical applications, in particular, for gold nanoparticle-based assays.

Introduction

The need for fast, cheap, and precise detection of DNA in samples of hair, blood, saliva, and other body fluids is increasing, both in medical and pharmaceutical applications as well as in forensic science. To meet these requirements, the research community is striving to develop new methods and assays that are highly specific, selective, and rapid. A clear trend in modern bioanalytics is to develop highly integrated and miniaturized biochip devices that can be produced in large quantities at a low cost. There exist today a huge number of promising optical transducer technologies that are being applied in DNA sensing, many of which utilize a solid support as the sensing substrate.[1−6] The supporting substrate may consist of a metal, a semiconductor, or an insulator in the form of a macroscopic surface or a suspension of colloidal particles. Gold is frequently used as a substrate material in biosensing, both as a macroscopic surface[6−10] and as a colloidal suspension.[11−17] In this work, we focus on the use of gold as a substrate material to study fundamental DNA base−substrate interactions. The aim of this work is to increase the understanding of how a DNA biosensor should be designed in the context of the choice of sensing layer, since earlier investigations, discussed below, show the importance of a properly composed molecular layer for optimized signal response and sensitivity. We have therefore investigated the interaction of the four bases with a thin polycrystalline gold film using temperature-programmed desorption−infrared reflection absorption spectroscopy (TPD-IRAS) and and temperature-programmed desorption−mass spectrometry (TPD-MS). Although previous attempts have been made to rank the binding strength of the individual bases to gold,[18−20] to our knowledge, this is the first detailed comparison of the structure and desorption dynamics of all four DNA bases.

Previous investigations of DNA fragment−gold interactions show that the binding of the four deoxynucleosides, dA, dC, dG, and dT, to gold nanoparticles differs mainly in the binding strength, with dT binding significantly weaker than that of the other three deoxynucleosides.[21] Moreover, in a study of thiol−oligonucleotide-modified gold nanoparticles, Demers and coworkers[22] showed that it was possible to achieve higher recognition strand loading, that is, a larger amount of molecules, on the particles using a spacer of thymidine (dT_{20}) instead of adenine (dA_{20}) between the thiol anchoring group and the functional oligonucleotide portion. They attributed this improvement to the weaker interaction between the (dT_{20}) spacer and the gold surface and to the formation of a smaller "footprint" of dT_{20} on the gold surface. However, particles loaded with oligonucleotides containing adenine spacers exhibited comparable or higher hybridization activity. Steel et al.[23] also showed a sequence-dependent behavior for modification of gold particles with thiol−oligonucleotides, where dT_{20} is compared with a mixed 20-mer oligonucleotide. These data suggested that it is

* Corresponding author. Phone: +46-13-281877. Fax: +46-13-288969. E-mail: bolie@ifm.liu.se.

10.1021/jp051617b CCC: $30.25 © 2005 American Chemical Society
Published on Web 07/14/2005

important to understand the interactions of bases with gold in order to tune oligonucleotide strand density and sterics and thus maximize the hybridization activity of biosensor surfaces.[21,22,24]

The adsorption behavior of single-stranded DNA to thin gold films also has been investigated, and the conclusions from these studies are in excellent agreement with the gold nanoparticle investigations above, that is, the thymine-containing oligonucleotides show the weakest interaction with the gold film.[25] Research on the structure of self-assembled DNA bases on metallic substrates previously has been published by several groups utilizing STM,[1,26−29] infrared and Raman spectroscopy,[30−32] or EELS.[1] Together, these studies show that the four bases, in general, spontaneously bind to macroscopic and colloidal metal substrates. The molecules bind either "belly-down" to the substrate or edge-on, or in an amorphous manner in well-defined 2D structures.

The combination of TPD-MS and TPD-IRAS provides a powerful tool for the study of dynamic events of molecular species on metal surfaces.[33−35] TPD-MS offers information about the desorption energies of the adsorbed species as well as about coverage, distribution, and population of different adsorption sites on the substrate surface. IRAS may be used to obtain complementary information about coverage as well as about the structure and orientation of the adsorbed species both at a pre-defined temperature and also during the course of the TPD experiment. Thus, one can follow the structural transitions occurring in the adsorbed layers prior to or during desorption and correlate these events to the MS signal. The main focus of this study is on adenine and guanine because they display the most interesting desorption behavior.

Experimental Section

Materials and Samples. The thin polycrystalline gold films used in the experiments were prepared by electron beam evaporation of 2000-Å gold (99.95%) on polished silicon (100) wafers precoated with a 25-Å-thick titanium adhesive layer. The evaporation was performed in a Balzer UMS 500P system operating at a base pressure of $\sim 5 \cdot 10^{-10}$ mbar and at an evaporation pressure of $\sim 10^{-7}$ mbar. The evaporation rates were 10 and 1 Å/s for gold and titanium, respectively. The gold samples were stored in plastic beakers until use. The samples were cleaned for 10 min in a 5:1:1 mixture of MilliQ water, 30% ammonia, and 25% hydrogen peroxide at 80 °C, followed by thorough rinsing in MilliQ water and drying in N_2 immediately before immersing them in the incubation solutions. All samples, unless otherwise stated, were incubated in thoroughly washed polypropylene vials (Nalgene) for 12 h using freshly prepared 50 μM solutions of the bases (Aldrich). Multilayer samples of the bases were prepared by putting a drop of a 50 μM solution on the gold surface and then allowing excess solvent to evaporate. The base solutions were prepared in MilliQ water; guanine solutions were also prepared in 50 μM ethanol−chloroform (50:50). Ethanol was purchased from Kemetyl, Haninge, Sweden, and chloroform from Merck.

Analytical Techniques. The TPD measurements were made in a custom-built vacuum system, with a base pressure of $5 \cdot 10^{-10}$ mbar. The TPD mass spectrometry (MS) and infrared (IR) data were acquired by increasing the substrate temperature from 25 to 250 °C, using a linear heating ramp $T = T_o + \beta t$. The mass spectrometry (MS) data were recorded using a HAL 301 Quadrupole Positive Ion Counter from Hiden Analytical mounted directly in front of the sample surface. The TPD-MS traces reported herein were recorded for the full masses corresponding to intact bases, that is, *m*/*e*: A = 136, G = 152, C = 111, T = 127; the full masses were chosen since no indication of fragmentation prior to desorption was evident (also see Supporting Information). Desorption energy was calculated using the equation published by Redhead,[36] assuming first order of desorption, a linear increase of the sample temperature (β = 0.25 K/s), and a vibrational pre-factor ν of 10^{13} s^{-1}.[37]

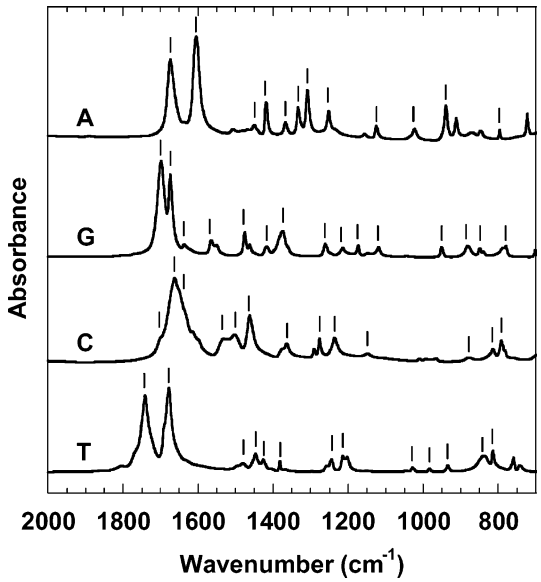

Figure 1. Isotropic spectra of the four bases homogenized in KBr. The absorption intensities are normalized for easier comparison. The labeled peaks are listed and tentatively assigned in Table 1.

The IR apparatus used was Bruker IFS PID 22 aligned at an angle of incidence of 83°, and spectra were recorded at a resolution of 2 cm^{-1}. The setup used is described in more detail elsewhere.[35] Two different types of reflection absorption (RA) spectra were recorded during the study. Low-noise spectra were obtained by averaging 500 interferograms (~7 min acquisition time). The low-noise, high-quality RA spectra were recorded for comparison purposes prior to the TPD measurements as well as before and after annealing at pre-selected substrate temperatures. Dynamic RA spectra were recorded continuously during TPD by averaging 20 interferograms. Each spectrum was acquired for 17 s, processed, and saved over 11 s such that each new spectrum represented a time span of 28 s. The dynamic experiment allowed us to follow the structural transitions occurring in the layer prior to as well as during the desorption process. To analyze possible intermediate states, in some cases, the temperature ramp was paused at a certain temperature, the sample cooled quickly to room temperature, and a low-noise spectrum recorded.

The isotropic IR spectra of the bases were recorded using KBr pellets (Ø =13 mm) prepared by mixing approximately 0.5 mg of the base with 300 mg of KBr (Merck). The mixture was carefully homogenized in an alabaster mortar, and the mixture was pressed into a pellet in a Perkin−Elmer pressure device at a pressure of 7 tons for 5 min. The KBr spectra were recorded in transmission mode using a Bruker IFS 48 spectrometer by averaging 100 scans at 4-cm^{-1} resolution.

Results and Discussion

Infrared Spectra of the DNA Bases. Figure 1 displays the isotropic transmission KBr spectra of the four DNA bases investigated in this work. These bulk spectra enabled us to understand the structural transitions that occur when each of the bases absorbs onto and desorbs from a gold surface. All four spectra display a series of sharp peaks of varying intensity

SCHEME 1: Stick Models of the DNA Bases and Coordinate System

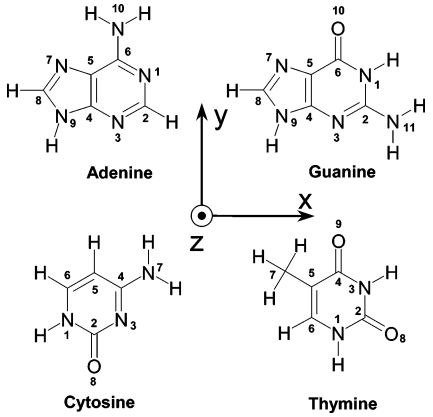

in the 700−2000-cm^{-1} region. The vast majority of these peaks originate from in-plane stretching and bending modes having transition dipole moments M_i's in the plane of the molecules (*x*, *y*, or *xy*, where either *x* or *y* may be the main contributor), Scheme 1. Some of them, however, belong to out-of-plane (*z*) modes, and they appear with variable intensity below 1000 cm^{-1}. The assignments of all the peaks in the KBr spectra shown in Figure 1 are not conclusive, primarily because of the complicated nature of the vibrational motions and the great number of possible intermolecular interactions occurring in the crystalline state. Indeed, several theoretical and experimental investigations report strongly diverging assignments.[38−48]

The 1800−1600-cm^{-1} region, for example, is particularly complicated because of a significant overlap between peaks belonging to in-plane C═C, C═N, C═O, and NH_2 stretching and bending modes. In this study we have chosen to follow the assignments reported in previous studies,[38,39,41−43,47,48] where assignments were based on spectra that closely resembled our own spectra with respect to peak position and relative intensities. The significant peaks are identified by ticks in Figure 1 and described by vibrational frequencies, transition dipole moments M_i's (in molecular coordinates, *x*,*y*,*z*), and tentative assignments in Table 1. We have combined these data with the surface dipole selection rule in IRAS (see the early works by Francis and Ellison[49] and Greenler[50]) to extract information about structural transitions and orientations of the bases on the gold substrate.

Even though the bases are structurally different, the overall intensity distribution of the peaks in the 700−2000-cm^{-1} region of the spectra displays many similarities. As mentioned before, strong features appear in the 1600−1800-cm^{-1} region, and they belong to in-plane ring, C═O, and NH_2 modes, respectively. Furthermore, a large number of in-plane ring, C−H, and N−H deformations can be observed in the region 1000−1500 cm^{-1}. In the case of adenine, for example, several of them are associated with M_i's in either the *x*- or *y*-direction, whereas only a few of them are of mixed character (*xy*), Table 1. The opposite applies for guanine and cytosine. It is also interesting to note that it is only the 797-cm^{-1} peak that can unambiguously be attributed to an out-of-plane (*z*) mode in the adenine spectrum. Moreover, the spectrum of isotropic adenine displays two strong well-resolved peaks at 1675 and 1604 cm^{-1}, respectively. These modes possess mutually orthogonal M_i's, a feature that later will be utilized to make predictions about the orientation of adenine on the gold surface.

For guanine the majority of peaks seen in Figure 1 are of mixed character. Only a few of them have the main component in the *x*- or *y*-direction. Three modes, however, are assigned to out-of-plane (*z*) modes, at 881, 850, and 780 cm^{-1}, respectively. Likewise, the vibrational modes of cytosine are generally of mixed character, except for the out-of-plane (*z*) modes at 815 and 792 cm^{-1}, respectively. The strong feature at ∼1660 cm^{-1} originates from several superimposed modes, creating a broad peak where the C═O stretching mode appears to be the main component. The spectrum of isotropic thymine is dominated by two equally strong peaks at 1742 and 1678 cm^{-1}, respectively, both of which originate from stretching modes of the carbonyl groups. These carbonyl groups also display out-of-plane deformation (*z*) that absorb at 839 cm^{-1}. The remaining

TABLE 1: Vibrational Frequencies, Tentative Assignments, and Direction of the Transition Dipole Moments (in molecular coordinates) for the Peaks Marked in Figure 1[a]

molecule	wavenumber (cm^{-1})	assignment	main direction of M_i
adenine[b]	1675	δ_{sc} NH_2	ip_y
	1606	ν N3−C4, C5−C6	ip_x
	1451	δ R5, R6	ip_y
	1419	δ R5, R6	ip_x
	1368	δ R5, R6	ip_y
	1334	δ R5, R6	$ip_{x(y)}$
	1309	δ R5, R6	ip_{xy}
	1252	δ R5, R6	ip_x
	1126	δ R5, R6	ip_{xy}
	1020	δ R5	ip_{xy}
	940	ν C8−N9	ip_x
	797	δ_{op} R5, R6	op_z
guanine[c]	1700	ν C═O, C5−C6	ip_y
	1675	δ_{sc} NH_2, ν C2−N11	ip_{xy}
	1638	δ_{sc} NH_2	ip_{xy}
	1566	δ R5, R6	ip_{xy}
	1476	δ R5, R6	ip_y
	1418	δ_{ip} N9−H	ip_{xy}
	1376	δ_{ip} N1−H	ip_{xy}
	1262	δ R5	ip_x
	1215	δ R5	ip_{xy}
	1174	δ R6	ip_x
	1120	δ R5	ip_{xy}
	951	δ R5	ip
	881	ω C═O, ω C2−N	op_z
	850	δ_{op} R6	op_z
	780	ω C═O, ω C2−N	op_z
cytosine[d]	1700 (sh)	δ_{sc} NH_2	ip_{xy}
	1663	ν C2═O	ip_y
	1640 (sh)	ν C5═C6	$ip_{x(y)}$
	1540	δ R6, N1−H	ip_y
	1503	δ_{sc} NH_2, C4−N7	$ip_{x(y)}$
	1463	δ ring	ip_y
	1364	δ_s N1−H, C5−H, C6−H	$ip_{x(y)}$
	1277	δ all H	ip_{xy}
	1237	δ R6	ip_{xy}
	1149	δ_s N7−H9, N7−H10	ip_{xy}
	878	δ R6	ip_{xy}
	815	δ_{op} R6	op_z
	792	δ_{op} R6	op_z
thymine[e]	1742	ν C2═O	$ip_{(y)x}$
	1678	ν C4═O, C═C	ip_y
	1482	δ_{ip} R6	ip
	1447	δ_{ip} N1−H	ip_x
	1427	δ_{as} C7−H	f
	1383	δ_{as} C7−H	f
	1245	δ R6	ip
	1215	ν C5−C7	$ip_{x(y)}$
	1029	δ R6	ip
	984	ω N−H	op_z
	935	ω C6−H	op_z
	839	ω C2═O, ω C4═O	op_z
	815	δ_{ip} R6, ω N1−H, C6H	op_z

[a] sh shoulder, δ deformation, ν stretch, ω wagging, sc scissoring, R5 five-membered ring, R6 six-membered ring, ip in the plane of the molecule. Index gives the main direction of the transition dipole moment in the coordinate system in Scheme 1. *x* mainly in the *x*-direction, *y* mainly in the *y*-direction, *y*(*x*) mainly in the *y*-direction with a component in the *x*-direction, *xy* mixed mode. [b] From refs 38 and 39. [c] From ref 41. [d] From refs 42 and 43. [e] From refs 47 and 48. [f] M_i is in a plane orthogonal to the plane of the molecule.

peaks originate from vibrational modes in the ring structure and C−H, N−H bond deformations, of which three are assigned to be out-of-plane (*z*) modes at 984, 935, and 815 cm^{-1}, respectively.

Mono- and Multilayer Formation on Gold. The purine and pyrimidine bases were adsorbed from solutions of water and/or ethanol/chloroform solutions to rapidly form monolayers on the surface of clean gold substrates. The distribution of the adsorbed bases analyzed via AFM has been reported before and is not repeated here.[19] In these studies, we used ellipsometry to define the conditions necessary for preparing about one monolayer of bases on the substrate and as a routine measure of average film thickness (data not shown). Other groups report the film thickness of DNA bases to fall in the 1−2-Å range[51] and that most of the bases self-assemble rapidly on Au(111) surfaces using ethanol as a solvent.[28] To determine the origin of peaks appearing in the TPD traces and RA spectra, we varied the thickness and coverage of the films by adjusting solution concentration, solvent, or incubation time. Multilayer layers were also prepared (>10 Å) for reference purposes, as described in the Experimental Section.

Desorption of Adenine Layers from Gold. The desorption behavior of adenine from gold was monitored using MS. Figure 2a shows the TPD-MS trace of the intact adenine molecules (m/e = 136) desorbing from a sample representing about a monolayer of adenine (RT). Three peaks appear, all of different strength and shape, suggesting that a multitude of adsorption sites exist for adenine on the gold surface. To be able to identify and investigate the peaks separately, a fresh adenine sample, prepared in the same way as RT, was inserted into the vacuum system. The substrate temperature of the sample was then increased at 0.25 K/s to 90 °C as indicated in Figure 2a, held at 90 °C for about 15−20 s, and then immediately cooled to room temperature. A normal TPD was subsequently performed on the sample, producing a MS trace of different appearance (A90) than the previous one (RT). The low-temperature peak is not present, while the main and high-temperature peaks appear largely unaffected. Another freshly prepared sample was inserted into the system, and the sample temperature was this time increased to 170 °C and rapidly cooled to room temperature. The MS trace from this TPD experiment (A170) again displays a different shape. Both the low-temperature peak as well as most of the main peak is absent in this trace. The only peak surviving is the high-temperature desorption peak at ∼210 °C and residues of the main peak (seen as a low-temperature tail on the 210 °C peak). These TPD experiments clearly show that there exist at least three different sites for adenine on the gold surface. In one site, adenine is loosely bound to gold, with a desorption peak at 90 °C, a temperature that is close to the peak desorption temperature of a multilayer of adenine desorbing from gold.[19] Thus, this low-temperature peak originates either from adenine molecules adsorbed on top of other adenine molecules (aggregates) or from adenine loosely bound to the gold substrate. The main desorption peak has its maximum at ∼170 °C, and the high-temperature peak is located at ∼210 °C. These peaks correspond to adenine adsorbed more tightly to the gold substrate. The low-temperature and high-temperature peaks are relatively sharp, suggesting that these sites are energetically well-defined, whereas the main peak is broad, most likely because of the coexistence of several overlapping sites. Such a distribution of energetically narrow adsorption sites may occur because we are doing experiments on polycrystalline gold surfaces that undoubtedly display point defects, steps, grain boundaries, and terraces of varying size and distribution. For the coverage of

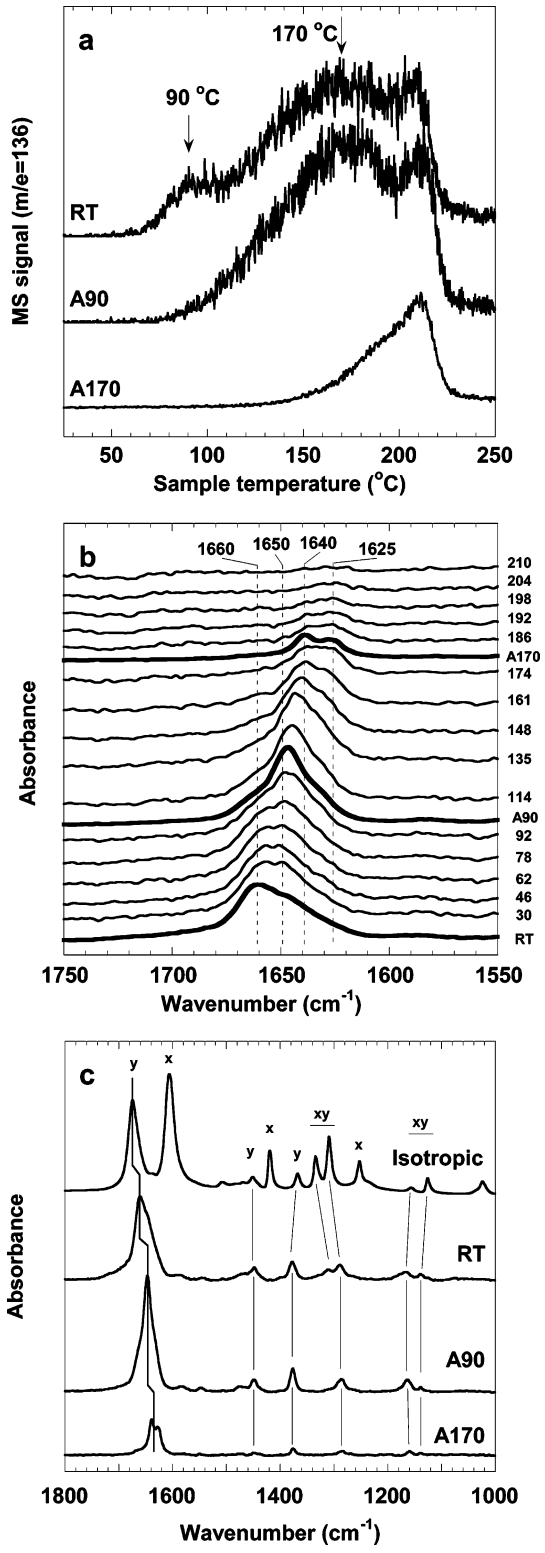

Figure 2. (a) TPD-MS traces of intact adenine molecules (m/e = 136) desorbing from gold. RT is the TPD trace of adenine adsorbed to gold without treatment, A90 is the TPD trace of adenine obtained after annealing at 90 °C, and A170 is obtained after annealing at 170 °C. All TPD-MS traces were obtained at a rate of 0.25 K/s by starting the ramping at room temperature. (b) RA spectra of adenine recorded during TPD. The spectra marked RT, A90, and A170 are low-noise spectra recorded after heating the sample to the temperature indicated; for more information see text. (c) Transmission spectrum of isotropic adenine in KBr and RA spectra of adenine on gold. The same nomenclature as in (b) applies. The inserted lines are introduced as a guideline to the eye. The main directions (*x*,*y*,*z*, and *xy*) of the M_i's (in molecular coordinates) are indicated along with the peaks.

TABLE 2: Observed TPD-MS Peak Temperatures and Calculated Desorption Energies for the Four Bases

	desorption peak temperature (°C)	desorption peak energy (kJ/mol)
adenine	90 ± 5	101 ± 1
	170 ± 10	124 ± 3
	210 ± 5	136 ± 2
guanine	180 ± 5	127 ± 2
	220 ± 5	139 ± 2
cytosine	160 ± 5	122 ± 2
thymine	100 ± 5	104 ± 2

the sample shown in the RT trace, the high- and low-temperature peaks contribute to approximately 5% each of the overall intensity, while the main peak contributes to the remaining 90%. In Table 2, we summarize the desorption energies (kJ/mol) for the peaks in Figure 2a. In the next section, we will use IR data to evaluate the various types of binding and/or reorganization phenomena that may also contribute to the complex nature of the MS trace and the broad peak at ∼170 °C.

Structure of Adenine Layers on Gold. IRAS was used to continuously monitor the structure and orientation of desorbing adenine. This experiment enabled us to follow the structural transitions occurring in the layers prior to or during the desorption event. Figure 2b displays how the TPD-RA spectra of approximately one monolayer of adenine on gold evolves in the 1750−1550-cm^{-1} region. The only feature seen in this region is a peak at ∼1660 cm^{-1} that is assigned to the NH_2 scissoring mode. This peak provided considerable information about how adenine absorbs to gold surfaces. At room temperature, the position of this peak is already shifted on gold compared to the position for isotropic adenine in KBr (1675 cm^{-1}). The peak is asymmetric with a tail extending into the low-frequency region, suggesting that it is composed of several modes representing different types of interactions with the gold substrate. It is observed in Figure 2b that the position and shape of this peak continuously changes during the course of the temperature ramp in the TPD experiment. The 1660-cm^{-1} peak displays three main characteristics during TPD: one in the RT−90 °C range, one in the 90−160 °C range, and a final one in the 160−210 °C range. The low-noise spectra of these characteristic states were recorded at room temperature after heat treatment at 90 and 170 °C, respectively, and are marked RT, A90, and A170 in Figure 2c. Note that we have inserted these low-noise spectra into the plot such that the A90 spectrum replaces the dynamic spectrum at 107 °C and A170 replaces the dynamic spectrum at 180 °C.[52]

The gradual change in peak position, shape, and intensity of the NH_2 scissoring mode may be due to several different interactions and orientations of adenine on gold, and it is most probably a combination thereof. Let us first assume that adenine is being adsorbed at different sites on the gold film. The peak is then built up from a set of vibrational modes representing the different sites of adenine on gold. The 1660-cm^{-1} peak, for example, shifts a few wavenumbers toward lower frequencies and loses intensity with increasing temperature before it finally disappears in the RA spectra obtained at 114 °C (only a tiny shoulder in present on a new peak at ∼1650 cm^{-1}). The 1660-cm^{-1} peak disappears in the same temperature interval as the first desorption maximum in the TPD-MS trace, Figure 2a, suggesting that it belongs to the loosely bound (aggregated) adenine molecules. The new peak at ∼1650 cm^{-1} can be seen already at 30 °C, and it grows continuously and becomes the dominating peak in RA spectra in the temperature range 90−160 °C. The peak shifts further ∼10 cm^{-1} to lower frequencies and increases in intensity (about a factor of 2) up to about 135 °C before it starts to decrease in intensity as adenine desorbs from the surface. Thus, the 1650−1640-cm^{-1} peak correlates very well to the main peak at 170 °C in the TPD-MS trace, Figure 2a. Two equally strong peaks appear at about 170 °C; the 1640-cm^{-1} peak and a new one at ∼1625 cm^{-1}. The 1640-cm^{-1} peak disappears as the temperature ramp continues, leaving the 1625-cm^{-1} peak as the only one remaining at 200 °C and above. We attribute the adenine molecules represented by the 1625-cm^{-1} peak to the high-temperature desorption peak seen in the TPD-MS trace at 210 °C. The exact origin of the 1625-cm^{-1} peak is at present not known, but a peak at 1629 cm^{-1} is also observed for an annealed monolayer sample of adenine on Cu(110)[1] (see below).

There is also a possibility that the adenine molecules continuously rearrange on the gold surface during the temperature increase because of increased mobility and spatial freedom, and these changes in how adenine interacts with the surface and neighboring molecules are reflected in the vibrational spectra. The gradual shift and intensity enhancement of the 1640-cm^{-1} peak clearly suggest that adenine reorganizes on the surface during the TPD experiment. For example, the orientation of the molecules may change, leading to a completely new intensity distribution of the peaks in the RA spectrum. The pure temperature dependence of the vibrational spectrum of adenine must also be taken into consideration. However, as the A90 and A170 spectra fit so well in the gradual change in the dynamic RA spectra, it is quite safe to conclude that the effects seen during TPD are not purely temperature-dependent, because the annealing experiments show that none of the observed spectral changes are reversible. Instead, the change is probably an effect of changing interaction with the substrate and/or surrounding molecules as the molecules desorb.

In Figure 2c, we compare the room-temperature RA spectrum (1800−1000 cm^{-1}) of adenine adsorbed from water solution onto gold with the isotropic KBr spectrum and the RA spectra of adenine on gold measured at room temperature after annealing at 90 and 170 °C, respectively. The RA spectrum (RT) is distinctively different from the isotropic spectrum, suggesting that either the adenine molecules are distorted in some way due to interactions with the surface or that some vibrational modes are absent because of a preferential orientation parallel to the substrate surface. The two strongest peaks in the isotropic KBr spectrum (1675 and 1606 cm^{-1}) are assigned to the NH_2 scissoring mode that is mainly in the *y*-direction and to an in-plane skeletal ring vibration mainly in the *x*-direction (see Table 1 and Scheme 1), respectively. In the RT monolayer spectrum, the in-plane skeletal ring vibration is almost completely missing (only a tiny feature can be seen). As the M_i of this skeletal ring vibration mode is mainly in the *x*-direction, the molecule appears to be preferentially oriented with the *x*-axis parallel to the gold surface. The NH_2 peak, however, appears as the dominating peak in the RA spectrum, suggesting that the molecule cannot be adsorbed flat, that is, with the *y*-axis aligned parallel to the gold surface. Instead, we propose that the *y*-axis (Scheme 1) is oriented at an angle with respect to the gold surface. The behavior of the other peaks confirms this orientation of adenine, that is, all three peaks that possess the main M_i in the *x*-direction (1606, 1419, and 1252 cm^{-1}) disappear when adenine is adsorbed to the gold substrate, whereas the peaks assigned to have their M_i's in the *y*-direction (1675, 1451, and 1368 cm^{-1}) are still present. A few other peaks in the spectrum that have their main M_i's in intermediate directions (*xy*) are visible, but they display a complex temperature behavior. The 1020-cm^{-1} peak is an exception though, raising certain doubts about its

SCHEME 2: Possible Orientations/Interactions of Adsorbed Adenine

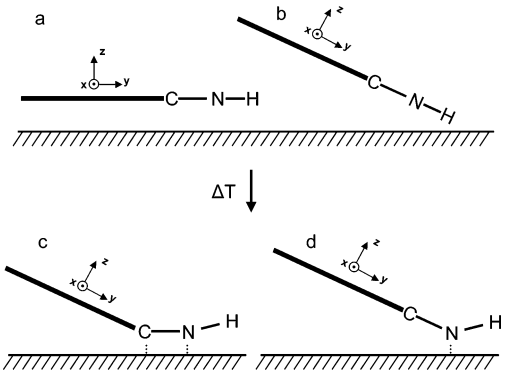

assignment to an in-plane *xy*-mode, Table 1. In fact, it appears to have a strong *x*-character.

When the samples are annealed at 90 and 170 °C, respectively, and subsequently cooled back to room temperature, the appearance of the peaks in the spectra changes. However, the general trend observed in the RT spectrum is still observed, that is, the peaks originating from vibrations in the *x*-direction are absent, whereas those with M_i's in the *y*-direction are still present. It is also observed that the frequencies and relative intensities of the peaks below 1600 cm^{-1} remain essentially unaffected upon annealing, suggesting that the general orientation of the adenine molecules does not change with increasing temperature, even though some of the molecules desorb. The main NH_2 peak, however, changes intensity, shape, and frequency during desorption, Figure 2b, as well as after annealing at 90 and 170 °C, Figure 2c. We find it hard to explain these spectral changes exclusively to a variation in molecular orientation of a planar adenine molecule on the gold surface. Instead, we believe that the complex behavior of the NH_2 peak reflects a gradual change in interaction with the gold surface, which is clearly supported by the appearance of several peaks in the MS trace, Figure 2a. A variety of different conformations of adenine on metal substrates previously have been discussed. Furukawa and co-workers[27] utilized STM to study adenine on Cu(111) and proposed a flat geometry, Scheme 2a. Such a conformation "belly-down" is not compatible with the observation of *y*-modes in the RA spectra, Figure 2c. Thus, if we assume that the adenine molecule adsorbs as a planar and intact entity on the gold surface, it must form an angle between the molecular plane (*y*-axis, Scheme 1) and the gold surface in order to make the *y*-modes visible, Scheme 2b. In their studies of adenine absorbed on Cu(110), Chen et al.[1] examined conformational models for either a flat "belly-down" or a distorted conformation via coordination through the NH_2 group. They concluded that the distorted conformation was the only one compatible with their high-resolution EELS data obtained after annealing the sample at 430 K (∼160 °C), and they reported a NH_2 scissoring peak at 1629 cm^{-1}. A downshift in the vibrational frequency for the NH_2 scissoring mode upon coordination to metal substrates or metal ions previously has been reported by other groups.[53,54]

Thus, coordination via the NH_2 group seems to explain what we observed for adenine on gold, at least at high temperature, because it allows for the NH_2 scissoring mode as well as the remaining *y*-modes at about 1450 and 1370 cm^{-1}, respectively, to appear in the spectrum at the same time as the *x*-modes cancel because of an unfavorable orientation parallel to the surface. It should be emphasized, however, that it is very difficult to explain the subtle details seen in the RA spectra of adenine on gold, Figure 2b,c. We believe, however, that the majority of adenine molecules initially adsorb as planar entities at RT according to Scheme 2b, perhaps with a small fraction of the adenine adopting the "belly-down" conformation, Scheme 2a. Raising the temperature using a constant ramping rate or to a predefined temperature (annealing) results in a gradual change in the way adenine molecules interact with the gold substrate as well as with neighboring adenine, resulting in the appearance of the distorted structure characterized by a NH_2 scissoring peak at 1625 cm^{-1}. The exact geometry of the species seen at high temperatures is not known. One possibility is that adenine coordinates to gold via both the C6 and N10 atoms, Scheme 2c. However, we would expect a parallel coordination of the C−N bond to influence the electronic structure of the ring structure and thereby the vibrational frequencies of the ring modes. This is definitely not the case. The ring modes (*y* and *xy*) seen below 1600 cm^{-1} do not change in frequency when comparing the RA spectra (RT, A90, and A170) in Figure 2c. Another possibility is that adenine coordinates through the amino group, thus changing the hybridization of the N10 atom from sp^2 (planar) to sp^3 (pyramidal), Scheme 2d. This distorted, nonplanar geometry is compatible with the disappearance of *x*-modes and the appearance of the NH_2 scissoring and the *y*-polarized ring modes at ∼1450 and 1380 cm^{-1}, Figure 2c. Note also that the peak position corresponding to the NH_2 scissoring mode for adenine on gold, 1625 cm^{-1}, is almost identical to the peak position observed for adenine coordinated through NH_2 to Cu(110).[1] We therefore propose that adenine forms a structure similar to that shown in Scheme 2d and that the MS peak at 220 °C is due to desorption of such species from the gold surface. One may argue that the *z*-modes also should appear in the RA spectra for the orientations suggested in Scheme 2. A problem though is that the *z*-modes often appear with very low and variable intensities, making them less useful for orientation analysis.

A remaining question to address is whether the site represented by the MS peak at 210 °C, Figure 2a, and the RA peak at 1625 cm^{-1}, Figure 2b,c, is formed because the molecules rearrange during TPD or if it is populated already in the virgin RT sample. If, for example, the A170 spectrum is subtracted from the RT spectrum, then we obtain a difference spectrum with sharp negative features in the 1640−1625-cm^{-1} region, suggesting that the high-temperature site is not present at full monolayer coverage (RT). Note, however, that a close to identical RA spectrum to that obtained after annealing at 170 °C (A170), Figure 2b,c, but with lower overall intensity (see Supporting Information), can be observed by adsorbing adenine to gold at low concentration (0.5 μM) and short time (30 min). We therefore have reason to believe that the 1625-cm^{-1} feature in Figure 2b,c represents a low-coverage site that appears because as adenine molecules desorb they leave more space for the remaining adenines to rearrange and coordinate to the gold surface via the NH_2 group.

Desorption of Guanine Layers from Gold. Since guanine is soluble only in water at low concentrations, we used both an ethanol/chloroform mixture as well as pure water as solvent for the incubation solutions. The MS traces of guanine desorbing from gold, Figure 3, reveal that guanine behaves very differently depending on the solvent and incubation time.

The topmost MS trace, marked (i), is from a multilayer of guanine desorbing as intact entities ($m/e = 152$) from a gold sample incubated for 12 h in a 50 μM (50:50 ethanol/chloroform) solution. The MS trace displays two peaks, one broad peak at 180 °C (127 kJ/mol) and a sharper and more intense peak at 220 °C (139 kJ/mol), indicating that guanine is

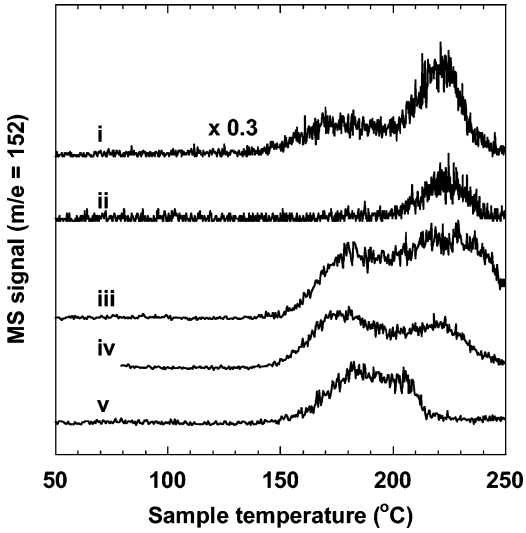

Figure 3. TPD-MS traces of intact guanine molecules ($m/e = 152$) desorbing from gold. (i) Trace for a sample prepared from ethanol/chloroform solution, (ii) trace for a solution cast and rapidly dried sample, and (iii), (iv), and (v) are traces obtained using water as a solvent. The incubation times were 180, 40, and 2 min.

adsorbed at two different sites when using ethanol/chloroform as a solvent. We also used TPD-MS to investigate how guanine desorbs from gold when the film is prepared by dropping a 1 mM ethanol/chloroform solution onto the surface followed by air-drying as well as by incubating in using aqueous solutions. Four different MS traces of guanine molecules desorbing as intact entities from gold are displayed in Figure 3 as follows: (ii) a solution cast 1 mM (50/50 ethanol/ chloroform) guanine solution and air-dried layer of guanine, and (iii−v) guanine layers formed in a 50 μM aqueous solution for 180, 40, and 2 min, respectively. The solution cast sample of guanine (ii) displays one single peak in the TPD-MS trace at ∼220 °C. The MS trace for the sample prepared from aqueous solution for 180 min (iii) displays two desorption peaks at approximately the same temperature as for the ethanol/chloroform sample. The high-temperature peak appears with reduced relative intensity as compared to the same peak in (i). When the incubation time is decreased, the intensity of the peak at 220 °C decreases even further, trace (iv), and it is finally completely missing in trace (v). The shoulder in trace (v) at about 200 °C appears from sites that cannot be resolved by IRAS and will therefore not be discussed here. These results confirm that guanine adsorbs at two different gold sites regardless of the solvent used. The loosely bound, low-temperature peak forms quickly upon adsorption of guanine on gold when using water as a solvent, see (v). Note, however, that the low-temperature peak is missing in the MS trace of the sample prepared by solution casting followed by rapid drying in air. We also observed (data not shown) that the high-temperature peak at 220 °C increases in intensity when we used higher concentrations or longer incubation periods to increase the guanine layer coverage. We therefore attribute the 220 °C peak to the multilayer peak, that is, from guanine molecules adsorbed on top of other guanine molecules, whereas the low-temperature peak is attributed to a phase consisting of a dispersed monolayer of guanine molecules on the gold surface. Thus, the TPD-MS data seem to suggest that the cohesive interaction(s) between guanine molecules are stronger than the adhesive interaction(s) with the gold substrate.

As for adenine, we used IRAS to continuously monitor the structure of guanine adsorbed to gold during the TPD experiments. The TPD-RA spectra recorded for a series of guanine

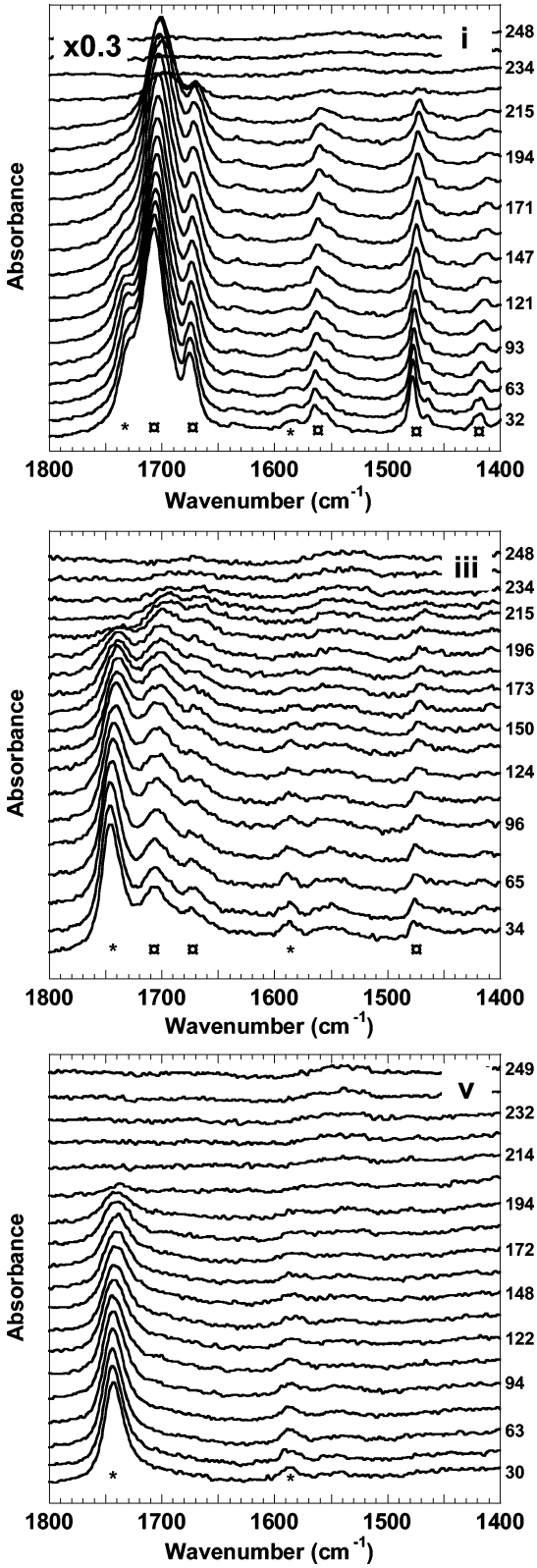

Figure 4. TPD-RA spectra of guanine on gold. The samples are prepared in three different ways; (i) from ethanol/chloroform, and from water during (iii) 180 and (v) 2 min of incubation. The peaks marked with * correspond to guanine bound directly to the substrate, while the peaks marked with ✚ correspond to solidlike guanine. The RA spectra in (i) are scaled by a factor of 0.3 for easier comparison.

samples are presented in Figure 4. The nomenclature is the same as the one given in Figure 3. The TPD-RA spectra for guanine adsorbed to gold from an ethanol/chloroform solution (i) display several strong peaks at about 1700, 1680, 1570, 1480, and 1420

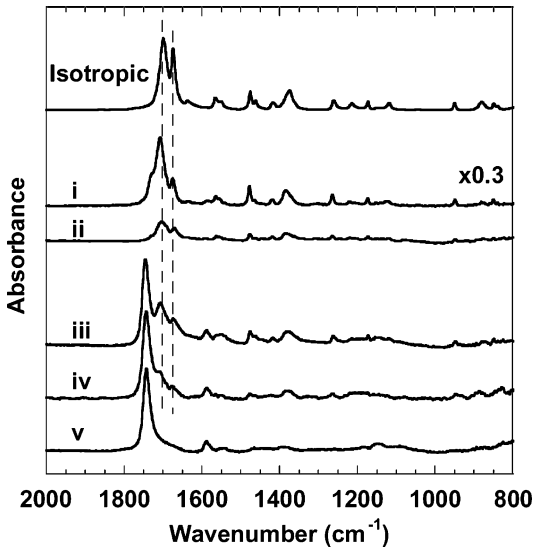

Figure 5. Infrared spectrum of isotropic guanine in KBr and RA spectra of adsorbed guanine, the same samples ((i)−(v)) as in Figure 3.

cm^{-1}, respectively, and they are labeled with ✚ in Figure 4. The same set of peaks can also be found in the isotropic KBr spectrum of guanine, and they can be undoubtedly assigned to crystalline guanine, Figures 1 and 5 and Table 1. These peaks appear with strong intensity up to about 200 °C when they start to rapidly disappear, and no such peaks can be seen in the TPD-RA spectra above 230 °C. This behavior correlates very well with TPD-MS data and supports our previous assignment of the 220 °C MS peak to be due to desorption from aggregated or multilayerlike guanine. Two additional peaks at 1745 and 1585 cm^{-1}, labeled with *, appear in the RA spectra (i). The 1745-cm^{-1} peak, a shoulder on the main 1700-cm^{-1} peak, and the 1585-cm^{-1} peak both disappear in the TPD-RA spectra before the multilayer peaks ✚ in (i), Figure 4. Both of these peaks become the most prominent ones in the RA spectra of guanine adsorbed onto gold from a water solution for 180 min (iii) or less, but note that the desorption order is still the same, that is, they disappear at significantly lower temperatures than those labeled with ✚ in (i) and (iii). The bottom panel (v) of Figure 4 shows the TPD-RA spectra of guanine adsorbed to gold from a water solution of guanine for 2 min. The only peaks seen are those at 1745 and 1585 cm^{-1}, suggesting that this spectrum represents a monolayer/submonolayer of guanine. Thus, we can attribute the low-temperature peak seen in the TPD-MS trace at about 180 °C to guanine desorbing from a monolayer/submonolayer phase on gold represented by the two peaks at 1745 and 1585 cm^{-1}. In contrast to the TPD-RA data for adenine, it is notable that the peaks seen in the RA spectra for guanine, multi- and monolayer peaks, do not change their shape or position during the course of the TPD experiment. While the spectra of adenine display a gradual change of shape as well as a shift in the position of the NH_2 scissoring mode with increasing substrate temperature, the only visible change in the RA spectra is the decrease in peak intensity as the molecules desorb. Taken together, our TPD-MS and TPD-IR data suggest that, at low coverage, guanine adsorbs onto a single site represented by two peaks in the RA spectra at 1745 and 1585 cm^{-1}, respectively, from which it later desorbs forming a low-temperature peak in the MS trace. Another site/phase is observed upon increasing the coverage consisting most likely of aggregates of different size and shape residing on top of the monolayer phase. Our infrared data agree excellently with the MS data, confirming that the cohesive forces between guanine molecules ($T_{des} \sim 220$ °C) in the aggregated phase are stronger than the adhesive interactions between guanine and gold ($T_{des} \sim 180$ °C).

Structure of Guanine Layers on Gold. Low-noise spectra of guanine adsorbed to the gold surfaces were also recorded prior to the TPD measurements described above, and these spectra are summarized in Figure 5 together with the isotropic KBr spectrum of guanine. The peaks seen in (i) and (ii) resemble those in the isotropic spectrum except for a few minor variations in peak positions and relative intensities. The peaks representing crystalline-like guanine are also present in the spectrum of guanine adsorbed to gold using water as a solvent when the incubation time is sufficiently long, that is, after 180 min in a 50 μM solution.

However, the crystalline peaks disappear upon lowering the coverage, and the 1745-cm^{-1} peak and the significantly weaker one at 1585 cm^{-1} become the only peaks seen when incubation time is shortened to 2 min. The 1745-cm^{-1} peak is attributed to a free, non-hydrogen bonded, carbonyl group. Kasende et al.[55] published data where they compare IR spectra of 9-methylguanine in the solid state and matrix-isolated in argon, and they observed a shift in the carbonyl peak of 9-methylguanine from 1684 cm^{-1} in the solid state to 1752 cm^{-1}/1741 cm^{-1} in the matrix-isolated form. This is in good agreement with the position observed for guanine at low coverage on gold (v), Figure 5, suggesting that guanine forms a dispersed monolayer phase on gold at low coverage where lateral interactions (hydrogen bonding) between neighboring molecules are unlikely to occur. The strong C═O stretching peak we observe at 1745 cm^{-1} (M_i parallel with the C═O axis) also suggests that the molecular plane of guanine (*y*-axis, Scheme 1) is nonparallel with the metal surface, thus ruling out the possibility of a flat "belly-down" conformation. Kasende et al.[55] also assigned a strong mode at 1622 cm^{-1} to the NH_2 scissoring vibration. This peak is absent in the guanine RA spectrum on gold (v), Figure 5, most likely because of an unfavorable (parallel) orientation on the gold surface. Although an analysis of the molecular orientation of guanine on gold is more complicated than for adenine because of the mixed character (*xy*) of many of the guanine modes, we can at least conclude that the strong C═O stretching peak appearing at 1745 cm^{-1} (*y*) supports a tilted orientation similar to that observed for adenine, Scheme 2b. However, on the basis of these data we do not expect guanine to form a strongly bound structure similar to the one suggested for adenine, Scheme 2d.

To summarize the observations so far for the purines on polycrystalline gold, we conclude that adenine forms a weakly bonded phase which is structurally identical to solid, crystalline adenine, and which also desorbs as a typical multilayer of aggregated adenine molecules, that is, the corresponding MS peak increases in strength with increasing coverage. At least two additional sites can be identified for adenine on gold where the adenine molecules are more strongly bound to the gold surface. One of these sites is attributed to a structure where the adenine molecule is coordinated to gold via the nitrogen atom in the NH_2 group, leading to a distorted (nonplanar) structure of adenine. The situation for guanine is different. The MS trace consists of two peaks representing a weakly bonded phase of dispersed guanine molecules and an aggregated phase that is more strongly bound to the surface. Thus, adhesive interactions seem to be responsible for the formation of a dispersed monolayer phase of adenine on gold, but interestingly, the cohesive interactions established between guanine molecules seem to form an even more stable structure of aggregated

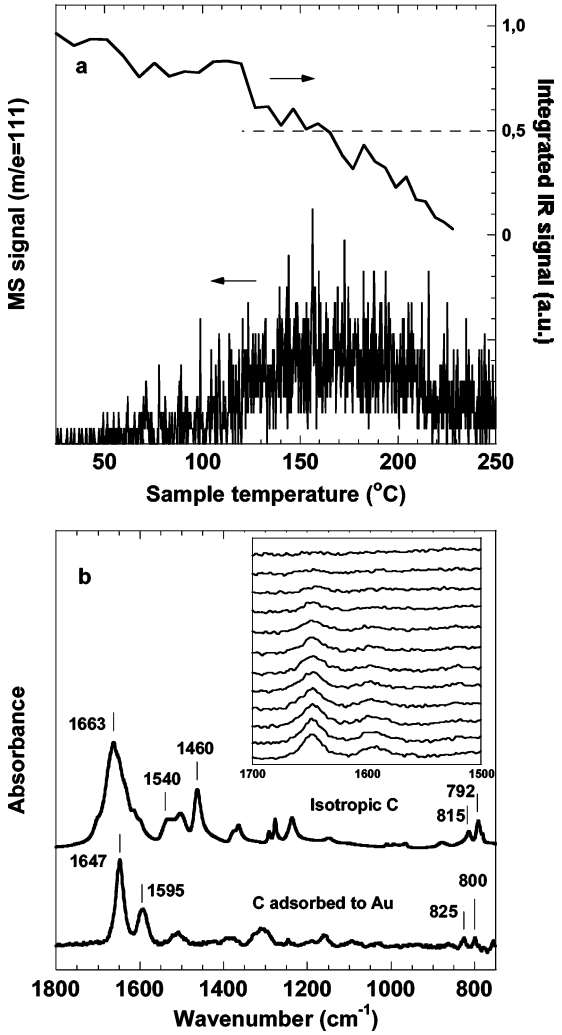

Figure 6. (a) TPD-MS trace of intact cytosine molecules ($m/e = 111$) desorbing from gold (lower panel). Integrated area (normalized) as a function of temperature of the main peak in the RA spectra (upper panel), see Figure 6b. The level at which 50% of the initially adsorbed cytosine molecules remain on the surface is indicated by the dotted line. (b) Transmission spectrum of isotropic cytosine in KBr and RA spectrum of adsorbed cytosine at a coverage corresponding to about one full monolayer. The inset shows TPD-RA spectra of cytosine on gold.

guanine molecules on gold. A way to confirm the desorption energies for adenine and guanine is through replacement experiments, presented in the Supporting Information.

Desorption of Cytosine Layers from Gold. The MS trace for intact cytosine molecules desorbing from gold is the lower plot in Figure 6a. The peak representing the full mass of cytosine ($m/e = 111$) is very weak. We utilized therefore the integrated area of the main IRAS peak, discussed below, to support the TPD-MS data. The upper plot in Figure 6a shows the correlation between the intensity of the main peak in the RA spectrum of cytosine and the substrate temperature. The level at which the RA peak intensity has decreased to 50% of its initial value correlates well with the peak desorption temperature $T_{des} \sim 160$ °C (122 kJ/mol) in the MS trace.[19] The MS desorption peak is broad and featureless though, making it hard to conclusively assign it to a peak representing a single site. However, TPD-RA spectra obtained for a monolayer of cytosine, in a similar way as for adenine and guanine (Figures 2b and 4), suggest that cytosine desorbs from a single site, that is, the frequency and shape of the main peaks at 1647 and 1595 cm^{-1} in the RA spectra remain the same throughout the desorption event, see inset Figure 6b.

Structure of Cytosine Layers on Gold. Figure 6b reveals significant differences between the RA spectrum of approximately one monolayer of cytosine and that of isotropic cytosine in KBr. Szczesniak et al.[43] have undertaken a thorough experimental and theoretical investigation of the infrared spectrum of cytosine in its polycrystalline state and in matrix isolation (argon and nitrogen). Cytosine exists in two tautomeric forms, amino−oxo and amino−hydroxy, of which the amino−oxo form is the dominating one in polycrystalline cytosine. Therefore, we combined their assignments for the amino−oxo form[43] with those presented by Santamaria et al.[42] to interpret our RA spectra. The main peak in the isotropic KBr spectrum at 1663 cm^{-1} is mainly due to the C═O stretching, Table 1. The frequency of this mode suggests that the C═O group is involved in hydrogen bonding to neighboring cytosine, because free C═O groups (matrix-isolated) are expected to absorb near 1710−1720 cm^{-1}.[43] The C═O mode (*y*) at 1663 cm^{-1} is not present in the RA spectrum. Nor can we observe any of the strong-to-medium intensity modes at about 1540 and 1460 cm^{-1} (also *y*), respectively, suggesting that the cytosine molecules are preferentially oriented with the *y*-axis aligned parallel to the gold surface, Scheme 1. However, two relatively strong peaks appear in the RA spectrum at 1647 and 1595 cm^{-1} along with a few less intense ones at 1506, 1313, 1160, 825, and 800 cm^{-1}, respectively. The 1647 and 1595 cm^{-1} modes, which appear as shoulders on the main peak in the isotropic KBr spectrum, are assigned to in-plane ring and NH_2 scissoring modes. These modes possess M_i's in the *x*-direction, Table 1, and the same applies for the modes at 1506, 1313, and 1160 cm^{-1}. Moreover, two out-of-plane modes seen at 815 and 792 cm^{-1} for isotropic cytosine are also visible in the RA spectrum, with a slight shift, at 825 and 800 cm^{-1}, respectively. Taken together, the absence of peaks due to free as well as hydrogen-bonded C═O groups suggests that the C═O bond (*y*-axis) of cytosine is aligned parallel to the gold surface. The appearance of both *x*- and *z*-modes reveals, however, that a flat orientation is unlikely. Instead we suggest a tilted orientation on the gold surface, similar to what we observed for the purines, Scheme 2b. This interpretation assumes that cytosine adsorbs on gold as a planar molecule.

Desorption of Thymine Layers from Gold. The lower plot of Figure 7a displays the TPD-MS trace of approximately a monolayer of intact thymine molecules desorbing from the sample surface. The signal is quite weak, as for cytosine, but it is relatively sharp and, most importantly, it appears at ∼100 °C (104 kJ/mol), that is, at a significantly lower temperature than for cytosine, adenine, and guanine. The desorption peak maximum agrees also with the temperature corresponding to the 50% value obtained from the RA spectrum, see the top plot in Figure 7a. These data suggest that thymine desorbs from a weakly bound, single site on the gold surface.

Structure of Thymine Layers on Gold. The plots in Figure 7b reveal that when thymine adsorbs onto gold, the infrared spectra change significantly compared to the isotropic spectrum of the crystalline state. In the RA spectrum, two major sharp peaks are seen at 1660 and 1605 cm^{-1}, respectively. These peaks as well as a few weaker ones near 1505, 1400, 1270, 1160, and 1100 cm^{-1} have no counterparts in the isotropic spectrum. The only peak seen in both spectra is the out-of-plane mode (*z*) near 810 cm^{-1}. This observation suggests that thymine is affected by the proximity to the metal surface and that the desorption peak seen at ∼100 °C cannot be interpreted as being due to

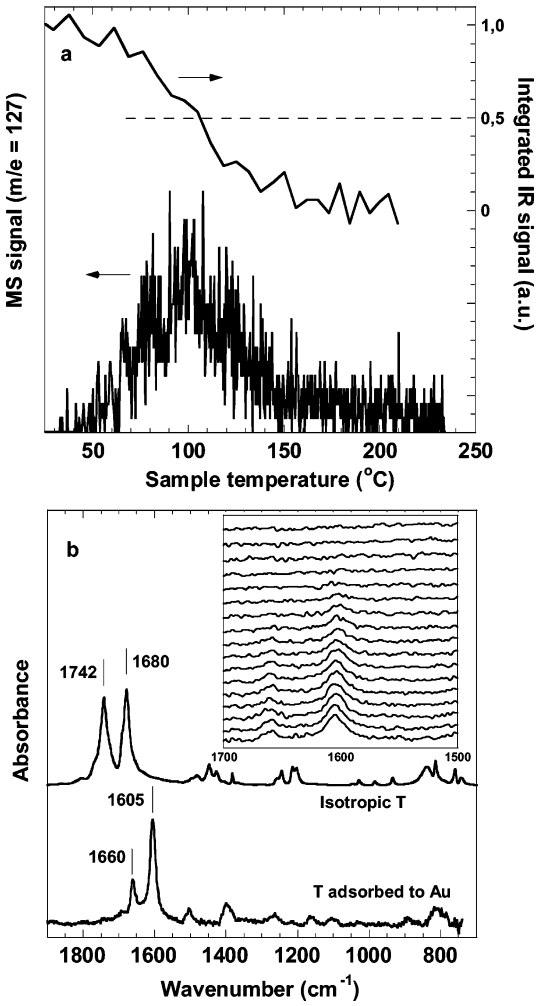

Figure 7. (a) TPD-MS trace of intact thymine molecules (m/e =127) desorbing from gold (lower panel). Integrated area as a function of temperature of the main peak in the RA spectra (upper panel), see Figure 7b. The level at which 50% of the initially adsorbed cytosine molecules remain on the surface is indicated by the dotted line. (b) Transmission spectrum of isotropic thymine in KBr and a RA spectrum of adsorbed thymine at a coverage corresponding to approximately one full monolayer. The inset shows TPD-RA spectra of thymine on gold.

multilayer desorption. Instead, we believe that the RA spectrum reflects a phase of dispersed, weakly bound thymine on the gold surface. Two strong peaks appear in the isotropic spectrum at 1742 and 1680 cm^{-1} that are attributed to C2═O and C4═O/C═C stretching vibrations, respectively.[48] These two peaks seem to shift, in parallel, to lower frequencies in the RA spectrum, most likely because of interactions with the gold substrate. Aroca et al.[30] used surface-enhanced Raman scattering (SERS) to investigate thymine in the solid state as well as on silver islands. They assigned the sharp and strong peak at 1672 cm^{-1} in the Raman spectrum of solid thymine to in-phase C4═O/C═C stretching modes. The corresponding C2═O mode is seen at 1742 cm^{-1} in the isotropic KBr spectrum, but it is not active in the Raman spectrum. The C4═O/C═C peaks shift from 1672 to 1597 cm^{-1} ($\Delta\nu = 75$ cm^{-1}) when thymine adsorbs on silver.[30] We observe an identical downward shift upon adsorption of thymine on gold (1680 to 1605 cm^{-1}), Figure 7a, suggesting that thymine interacts with gold and silver similarly, most likely through direct coordination to the surface via the carbonyl oxygen and possibly also via the nitrogen atoms. The origin of the 1660-cm^{-1} peak is not as straightforward as for 1605-cm^{-1} peak. One possibility is that the 1660-cm^{-1} peak in the RA correlates to the 1680-cm^{-1} peak in the isotropic spectrum, which is only marginally shifted because of weak interactions with the surface. We expect, in this case, to observe two structurally different populations of thymine on the gold surface: one that interacts strongly with gold (1605 cm^{-1}) and another one that interacts less strongly (1660 cm^{-1}). Since we observe only a single peak in the MS trace, this explanation is less likely. In this case, we would also need to explain why the C2═O peak at 1742 cm^{-1} is absent in the RA spectrum, Figure 7b, and this is not an easy task considering the possibility of having at least two different structures of thymine molecules on the gold surface.

Another possibility is that the both the C4═O and the C2═O groups, and perhaps also the amino groups, are involved in the binding to the surface (although weak) and that the 1660-cm^{-1} peak appears because of a downward shift of the 1742-cm^{-1} peak. A flat "belly-down" orientation would allow thymine to interact simultaneously with gold via the two carbonyl oxygen. A flat orientation, however, is not compatible with the appearance of in-plane modes (x or y) in the RA spectrum, making a tilted orientation of the plane of the ring more likely. We conclude also from TPD-RA experiments that the 1660 and 1605-cm^{-1} peaks originate from a single structural element of thymine molecules on the gold surface because there is no change in the relative ratio between the 1660 and the 1605-cm^{-1} peaks as a function of temperature, see inset in Figure 7b, but rather the peaks disappear simultaneously as the intact thymine molecules desorb from the substrate.

The pyrimidines display a less complicated desorption behavior compared to the purines. The thymine TPD-MS trace shows a single narrow peak representing desorption from a loosely bound and dispersed monolayer phase on gold. The cytosine desorption peak is broader than the one observed for thymine, and most importantly it appears at significantly higher temperature. The trends observed here confirm our earlier ranking of the adhesive interactions between the four DNA bases and gold[19] and provide at the same time a more detailed picture about the molecular mechanisms responsible for the adhesive forces. Replacement experiments in order to confirm the relative desorption energies of the bases adsorbed to gold are presented in the Supporting Information.

Conclusions

The work presented in this paper shows that the DNA bases bind to polycrystalline gold in a highly complex manner, with each base behaving differently on the surface. Adenine desorbs over a fairly broad range of temperatures with a desorption maximum near 170 °C, corresponding to a desorption enthalpy of 124 kJ/mol. According to IRAS data, the small fraction that desorbs at 210 °C are NH_2-coordinated and distorted, nonplanar molecules. Because of its similarity to the peak observed for multilayer samples of adenine, the low-temperature peak, which varies in intensity depending on coverage, undoubtedly corresponds to aggregated adenine. Thus, the adhesive interactions with the gold determine the desorption energy and thereby the stability of the adenine overlayer. The situation is very different for guanine. Two different phases coexist simultaneously on gold for a sample corresponding to approximately one monolayer of guanine: a dispersed phase of oriented guanine molecules that is structurally very different from solid guanine, and a phase consisting of aggregated, solidlike guanine. The dispersed phase of oriented molecules desorbs first, at about 180 °C (127 kJ/mol), that is, at approximately the same temperature as the adenine molecules, whereas aggregated

guanine desorbs at a higher temperature, ~220 °C (139 kJ/mol). This observation undoubtedly shows that the cohesive forces are more important than the adhesive forces for obtaining a stable overlayer of guanine on gold.

For monolayer samples, cytosine and thymine desorb from gold in a less complicated manner. In the MS trace of cytosine, a single desorption peak is seen at 160 °C (122 kJ/mol). Thymine also desorbs as a single peak but at a significantly lower temperature, 100 °C (104 kJ/mol). Both cytosine and thymine form dispersed phases on gold that are structurally very different from those observed in the solid state.

The infrared analysis shows that none of the four DNA bases adsorb on gold in an orientation where the plane of the ring(s) is perfectly parallel to the gold surface because they all exhibit in-plane vibrations in their RA spectra. Instead, all four molecules appear to be oriented with the molecular plane at an angle with respect to the gold surface. This result is somewhat surprising considering the huge amount of STM data suggesting a flat orientation on single-crystalline supports. On the other hand, a tilt is not always resolved in the topographic STM images. Note also that we are not suggesting perpendicularly "edge" oriented ring structures for the bases.

The data we present explain previous observations that spacers of weakly interacting thymine residues near the anchoring site (for example, SH) in single-stranded oligonucleotides result in higher surface coverages whereas adenine spacers lower the oligonucleotide surface coverage but can provide additional stability to colloidal particles. From the perspective of biosensor applications, this detailed information about how the DNA bases interact with gold surfaces will enable researchers to improve the stability and activity of oligonucleotide capture layers.[21−25]

Acknowledgment. This study was supported by the Swedish Foundation for Strategic Research (SSF) through the Biomimetic Materials Science program, and by the Swedish Research Council (VR). C.A.M. acknowledges the NSF, AFOSR, and DARPA for support of his research, and L.D. thanks NSERC (Canada) for fellowship support.

Supporting Information Available: Exchange of DNA bases on gold, correlation of RA and MS data, and low-coverage RA data for adenine. This material is available free of charge via the Internet at http://pubs.acs.org.

References and Notes

(1) Chen, Q.; Frankel, D. J.; Richardson, N. V. *Langmuir* **2002**, *18*, 3219.
(2) Bailey, R. C.; Nam, J. M.; Mirkin, C. A.; Hupp, J. T. *J. Am. Chem. Soc.* **2003**, *125*, 13541.
(3) Jelen, F.; Yosypchuk, B.; Kourilova, A.; Novotny, L.; Palecek, E. *Anal. Chem.* **2002**, *74*, 4788.
(4) Patolsky, F.; Katz, E.; Bardea, A.; Willner, I. *Langmuir* **1999**, *15*, 3703.
(5) Elghanian, R.; Storhoff, J. J.; Mucic, R. C.; Letsinger, R. L.; Mirkin, C. A. *Science* **1997**, *277*, 1078.
(6) Frederix, F.; Bonroy, K.; Laureyn, W.; Reekmans, G.; Campitelli, A.; Dehaen, W.; Maes, G. *Langmuir* **2003**, *19*, 4351.
(7) Riepl, M.; Enander, K.; Liedberg, B.; Schaferling, M.; Kruschina, M.; Ortigao, F. *Langmuir* **2002**, *18*, 7016.
(8) Sirkar, K.; Revzin, A.; Pishko, M. V. *Anal. Chem.* **2000**, *72*, 2930.
(9) Li, Y. J.; Ma, B. L.; Fan, Y.; Kong, X. G.; Li, J. H. *Anal. Chem.* **2002**, *74*, 6349.
(10) Veiseh, M.; Zareie, M. H.; Zhang, M. Q. *Langmuir* **2002**, *18*, 6671.
(11) Maxwell, D. J.; Taylor, J. R.; Nie, S. M. *J. Am. Chem. Soc.* **2002**, *124*, 9606.
(12) Velev, O. D.; Kaler, E. W. *Langmuir* **1999**, *15*, 3693.
(13) Liu, J. W.; Lu, Y. *J. Am. Chem. Soc.* **2003**, *125*, 6642.
(14) Mirkin, C. A. *Inorg. Chem.* **2000**, *39*, 2258.
(15) Mucic, R. C.; Storhoff, J. J.; Mirkin, C. A.; Letsinger, R. L. *J. Am. Chem. Soc.* **1998**, *120*, 12674.
(16) Storhoff, J. J.; Elghanian, R.; Mucic, R. C.; Mirkin, C. A.; Letsinger, R. L. *J. Am. Chem. Soc.* **1998**, *120*, 1959.
(17) Cao, Y. W.; Jin, R.; Mirkin, C. A. *J. Am. Chem. Soc.* **2001**, *123*, 7961.
(18) Boland, T.; Ratner, B. D. *Proc. Natl. Acad. Sci. U.S.A.* **1995**, *92*, 5297.
(19) Demers, L. M.; Ostblom, M.; Zhang, H.; Jang, N. H.; Liedberg, B.; Mirkin, C. A. *J. Am. Chem. Soc.* **2002**, *124*, 11248.
(20) Gourishankar, A.; Shukla, S.; Ganesh, K. N.; Sastry, M. *J. Am. Chem. Soc.* **2004**, *126*, 13186.
(21) Storhoff, J. J.; Elghanian, R.; Mirkin, C. A.; Letsinger, R. L. *Langmuir* **2002**, *18*, 6666.
(22) Demers, L. M.; Mirkin, C. A.; Mucic, R. C.; Reynolds, R. A.; Letsinger, R. L.; Elghanian, R.; Viswanadham, G. *Anal. Chem.* **2000**, *72*, 5535.
(23) Steel, A. B.; Herne, T. M.; Tarlov, M. J. *Anal. Chem.* **1998**, *70*, 4670.
(24) Jin, R. C.; Wu, G. S.; Li, Z.; Mirkin, C. A.; Schatz, G. C. *J. Am. Chem. Soc.* **2003**, *125*, 1643.
(25) Kimura-Suda, H.; Petrovykh, D. Y.; Tarlov, M. J.; Whitman, L. J. *J. Am. Chem. Soc.* **2003**, *125*, 9014.
(26) Tanaka, H.; Nakagawa, T.; Kawai, T. *Surf. Sci.* **1996**, *364*, L575.
(27) Furukawa, M.; Tanaka, H.; Kawai, T. *Surf. Sci.* **1997**, *392*, L33.
(28) Boland, T.; Ratner, B. D. *Langmuir* **1994**, *10*, 3845.
(29) Tao, N. J.; Derose, J. A.; Lindsay, S. M. *J. Phys. Chem.* **1993**, *97*, 910.
(30) Aroca, R.; Bujalski, R. *Vib. Spectrosc.* **1999**, *19*, 11.
(31) Ataka, K.; Osawa, M. *J. Electroanal. Chem.* **1999**, *460*, 188.
(32) Sanchez-Cortes, S.; Garcia-Ramos, J. V. *Surf. Sci.* **2001**, *473*, 133.
(33) Valiokas, R.; Ostblom, M.; Svedhem, S.; Svensson, S. C. T.; Liedberg, B. *J. Phys. Chem. B* **2000**, *104*, 7565.
(34) Valiokas, R.; Ostblom, M.; Svedhem, S.; Svensson, S. C. T.; Liedberg, B. *J. Phys. Chem. B* **2002**, *106*, 10401.
(35) Engquist, I.; Lundstrom, I.; Liedberg, B. *J. Phys. Chem.* **1995**, *99*, 12257.
(36) Redhead, P. A. *Vacuum* **1962**, *12*, 203−211.
(37) The Redhead equation for first-order desorption is used for calculating the desorption energies: $E = RT\ln((\nu T/\beta) - 3.51)$, where T is the desorption peak, R is the Avogadro constant, and ν and β are described in the text.
(38) Nowak, M. J.; Lapinski, L.; Kwiatkowski, J. S.; Leszczynski, J. *J. Phys. Chem.* **1996**, *100*, 3527.
(39) Giese, B.; McNaughton, D. *J. Phys. Chem. B* **2002**, *106*, 101.
(40) Florian, J.; Baumruk, V.; Leszczynski, J. *J. Phys. Chem.* **1996**, *100*, 5578.
(41) Florian, J. *J. Phys. Chem.* **1993**, *97*, 10649.
(42) Santamaria, R.; Charro, E.; Zacarias, A.; Castro, M. *J. Comput. Chem.* **1999**, *20*, 511.
(43) Szczesniak, M.; Szczepaniak, K.; Kwiatkowski, J. S.; Kubulat, K.; Person, W. B. *J. Am. Chem. Soc.* **1988**, *110*, 8319.
(44) Szczepaniak, K.; Szczesniak, M. M.; Person, W. B. *J. Phys. Chem. A* **2000**, *104*, 3852.
(45) Subramanian, V.; Chitra, K.; Venkatesh, K.; Sanker, S.; Ramasami, T. *Chem. Phys. Lett.* **1997**, *264*, 92.
(46) Aida, M.; Kaneko, M.; Dupuis, M.; Ueda, T.; Ushizawa, K.; Ito, G.; Kumakura, A.; Tsuboi, M. *Spectrochim. Acta, Part A* **1997**, *53*, 393.
(47) Aamouche, A.; Ghomi, M.; Coulombeau, C.; Grajcar, L.; Baron, M. H.; Jobic, H.; Berthier, G. *J. Phys. Chem. A* **1997**, *101*, 1808.
(48) Zhang, S. L.; Michaelian, K. H.; Loppnow, G. R. *J. Phys. Chem. A* **1998**, *102*, 461.
(49) Francis, S. A.; Ellison, A. H. *J. Opt. Soc. Am.* **1959**, *49*, 131.
(50) Greenler, R. G. *J. Chem. Phys.* **1966**, *44*, 310.
(51) Kawai, T.; Tanaka, H.; Nakagawa, T. *Surf. Sci.* **1997**, *386*, 124.
(52) The reason the two spectra replace the dynamic spectra at a temperature higher than the stop-temperature is that the cooling process is relatively slow. Thus, these samples will be annealed for a slightly longer time at elevated temperatures, driving the structural changes further than for a sample examined by dynamic TPD-IRAS.
(53) Mateo Marti, E.; Methivier, C.; Dubot, P.; Pradier, C. M. *J. Phys. Chem. B* **2003**, *107*, 10785.
(54) Johnson, D. F.; Wang, Y. Q.; Parmeter, J. E.; Hills, M. M.; Weinberg, W. H. *J. Am. Chem. Soc.* **1992**, *114*, 4279.
(55) Kasende, O. E.; Szczepaniak, K.; Person, W. B.; ZeegersHuyskens, T. *J. Mol. Struct.* **1997**, *435*, 17.